IMPACT OF TEMPORAL DOPPLER ON CSAS IMAGERY

Herter Ulrich[a], Bonnett Blair[a], Schmaljohann Holger[b], Fickenscher Thomas[a]

[a] Helmut Schmidt University, Holstenhofweg 85, Hamburg, Germany
[b] Bundeswehr Technical Center for Ships and Naval Weapons, Maritime Technology and Research (WTD 71), Berliner Str. 115, 24340 Eckernförde, Germany

Herter Ulrich, Helmut Schmidt University, Holstenhofweg 85, Hamburg, Germany, fax: +49 (0)40 6541-2061, ulrich.herter@hsu-hh.de

Abstract: *Circular Synthetic Aperture Sonar (CSAS) coherently processes acoustic data acquired along a circular trajectory. One usual approximation applied is the stop-and-hop assumption (SHA) and, in particular, the assumption that the antennas are motionless during transmission and reception, i.e. the impact of temporal Doppler is ignored. However, in reality, for a particular ping half of the insonified area of a CSAS image centred around the point of rotation experiences pulse contraction while the other half experiences pulse dilatation. This phenomenon of temporal Doppler is incorporated into the simulation of raw data of point scatters for circular paths of a single transmitter multiple-receiver array. Results for images processed in time domain either with or without compensation of the temporal Doppler effect in the received signal are contrasted with each other. Comparative evaluation of the degradation is presented based on the shift and 6dB peak width of the point spread function (PSF) with the object locus, centre frequency, bandwidth, and pulse length as parameters. The errors caused by uncompensated temporal Doppler are compared with those caused by the SHA. Compensation of Doppler cell migration on CSAS data is presented and discussed.*

Keywords: *CSAS, temporal Doppler, Doppler distortion, Doppler compensation*

1. INTRODUCTION

Circular Synthetic Aperture Sonar (CSAS) provides higher resolution images as compared to strip-map SAS. This level of image quality makes the technique more vulnerable to imaging errors and approximations like the stop-and-hop assumption (SHA) or uncompensated temporal Doppler in the processing algorithms [1, 2]. Migrating the processing based on SHA to a model that incorporates the effect of platform motion – in the following called non-SH or without SHA – requires the compensation of geometric distortion due to range dependent platform motion between transmission and reception (in the following called intra-ping platform motion) and temporal Doppler distortion due to platform motion during transmission and reception. The impact of intra-ping platform motion on CSAS imagery has been investigated and a compensation algorithm proposed [3]. The impact of temporal Doppler will cause both, geometrical distortion and image defocus. For the case of circular apertures this will be subject of this paper. In essence the nature of both effects is the same; it is a time-domain compression or dilatation of the signal throughout the ping period. However, during the transmission and reception intervals of the pulse a Doppler frequency shift and a compression or dilatation of the envelope of the pulse is observed which – if uncompensated in the processing – will result in a shift of the peak of the matched filtered signal in conjunction with a loss of peak magnitude and a peak broadening.

For the case of linear trajectories the impact of temporal Doppler on SAS imagery has been studied in detail [4, 5]. The wideband ambiguity function for linear FM (LFM) and Hyperbolic FM (HFM) chirped pulse signals was developed based on the assumption that the Doppler-scale factor η is constant over the two-way travel time of the pulse. A detailed analysis of target migration in the range/cross-range plane due to the intra-ping motion of the platform is presented in [5]. Knowing the trajectory of the platform as well as the platform-to-target geometry, geometric distortion as well as temporal Doppler distortion can be corrected during processing. For a linear trajectory compensation of temporal Doppler distortion in the (ω, k_u)-domain [4] as well as in the time-domain [5] has been proposed. The use of Doppler compensation is desirable as any residual phase error due to uncompensated Doppler is likely to cause a bias in any autofocus algorithm. On the other hand, DPCA timing errors due to uncompensated Doppler are expected to be smaller than the residual phase centre errors after bulk phase centre correction [4].

In [3] the impact of SHA on CSAS imagery has been investigated by simulations. Data that have been collected from a moving platform were processed under the SHA. However, signal compression or dilatation due to temporal Doppler was not included in the simulated raw data. The shift of the peak and the degradation of the 6dB width of the point spread function (PSF) – compared to the case where the data have been collected under SHA – were analysed with the object locus, radius of mission, and platform speed as parameters. Unlike for linear trajectories in the case of circular trajectories not only a geometric distortion is apparent but also image blurring. Therefore, a compensation scheme for circular trajectories was presented to mitigate the impact of intra-ping platform motion when processing under SHA. It is certainly interesting to compare those findings with those where the temporal Doppler effect is incorporated into the process of data collection. In this paper we investigate the impact of uncompensated temporal Doppler for processing with SHA. The tangential shift and degradation of the 6dB width of the point spread function (PSF) due to the impact of temporal Doppler are analysed with the object locus, centre frequency, bandwidth, and pulse length as parameters. Furthermore, the results of [4] are transferred to a compensation scheme for

temporal Doppler distortion in the case of circular trajectories. Finally, the errors caused by uncompensated temporal Doppler are compared to those caused by the SHA.

2. MODELLING THE IMPACT OF TEMPORAL DOPPLER ON LFM SIGNALS

2.1. SYNTHETIC RAW DATA

A time-domain CSAS simulator for pulsed LFM signals is used to generate artificial raw data of point scatterers for circular paths of a single transmitter multiple-receiver array. The apertures of individual transducers are assumed to be of rectangular shape with their according theoretical beam patterns. The time-domain scaling due to the temporal Doppler effect is described by the Doppler scale-factor η with

$$\eta = \frac{c+v_{r,Rx}}{c-v_{r,Tx}} \tag{1}$$

where c is the speed of sound and $v_{r,Tx}$ and $v_{r,Rx}$ are the relative platform speeds in the direction of the scatterer seen from the locations of the transmitter at the time of the begin of the transmitted chirp and of the receiver at the time of the begin of the received chirp, defined positive for decreasing range ($\eta > 1$) and negative for increasing range ($\eta < 1$). The values of $v_{r,Tx}$ and $v_{r,Rx}$ and, thus, η are approximated as constant values for each ping-scatterer-receiver triplet. Ignoring the round-trip delay and amplitude scale factors the received echo $e(t)$ of the wideband transmit signal $p(t)$ distorted by the temporal Doppler effect is

$$e(t) = p(\eta t) \ . \tag{2}$$

For a LFM chirped pulse signal the distorted chirp has a new pulse length $T' = \eta T$, new carrier frequency $f_0' = \eta f_0$, new bandwidth $B' = \eta B$, and new chirp rate $K' = \eta^2 K$ (where the respective variables without a prime refer to the nominal transmitted pulse) [4, 5]. With the travel times calculated for each ping-scatterer-receiver triplet, the LFM signals are delayed, weighted individually for all receive (Rx) array elements by the transducer beam-patterns according to their respective aspect angles, and summed up over all scatterers. A navigation file with emulated navigation data is generated in addition.

2.2. PROCESSING AND TEMPORAL DOPPLER COMPENSATION

For each ping the echos are beam-formed accounting for the nominal carrier frequency f_0 using a time-domain (back-projection) near-field r-φ-beam-former in ground range plane with the approximation of rectangular shaped array patterns (cut off at 3dB points of the transducer beam patterns). Hereafter the beamformed data are downconverted to baseband (BB) using the nominal carrier frequency f_0 and are range compressed with optional Doppler compensation accounting for a beam angle θ dependant Doppler scale-factor η. The beam angle θ considered for the Doppler compensation refers to the centre of the phase centres of the physical aperture for the particular ping. Range compression is performed computational efficient in the temporal-frequency domain by a multiplication of the spectrum of the received signal with the conjugate complex spectrum of the temporal Doppler shifted pulsed chirp. The

Parameter	Symbol	Value
Receiver spacing	Δ	2.5 cm
Carrier frequency	f_0	50 kHz / 75 / 100 kHz
Horizontal opening angle, null-to-null	θ	90° / 60° / 45°
Bandwidth	B	30 kHz / 60 kHz
Pulse duration	T	10 ms / 20 ms
Sound speed	c	1500 ms^{-1}
Radius of trajectory	R	30 m
Radius of full view area	R_f	12.1 m / 8.2 m / 6.2 m
Puls repetition period (PRP)	T_{prp}	200 ms
Platform speed	v	1.5 ms^{-1}
Height over ground	h	10 m
Processing beamwidth	θ_b	45° / 30° / 22.5°
Image grid resolution	$\Delta x = \Delta y$	1.50 mm
Theoretical resolution at central point [6, 7]	Δx_{theo}	1.2 cm

Table 1: Simulation and processing parameters.

spectrum $S'(\omega)$ of a Doppler distorted signal can be evaluated from the spectrum $S(\omega)$ of the undistorted signal as follows:

$$S'(\omega) = \frac{1}{\sqrt{\eta}} S\left(\frac{f}{\eta} - (\eta - 1)f_0\right). \tag{3}$$

For computational efficiency the Doppler shift $\Delta f = (1 - \eta)f_0$ is applied to the matched data before interpolation on ground plane followed by an upconversion to passband (PB) accounting for the nominal carrier frequency f_0 and subsequent azimuth compression. To avoid aliasing effects, a resolution finer than the minimum theoretical resolution for the central point, based on the carrier frequency [6], was chosen for the image grid.

3. SIMULATION RESULTS

In this section, the temporal Doppler effect on CSAS imagery with an up-chirp LFM waveform is assessed. Table 1 provides an overview over the simulation and processing parameters. In particular the impact of carrier frequency and bandwidth as well as pulse length is considered. In order to separate the temporal Doppler effect from the impact of intra-ping platform motion we investigate a scenario where both, data collection and processing, are performed under SHA. As quality metrics, the maximum 6dB peak width of the PSF was chosen. This was performed by: 1. searching for local maxima, 2. refining the positions by fitting Gaussian curves in radial and azimuthal directions, 3. interpolating image data along 100 azimuthal directions with the peak position as origin, and 4. fitting Gaussian curves to the azimuthal data to determine the 6dB peak widths and find the maximum width over all azimuths.

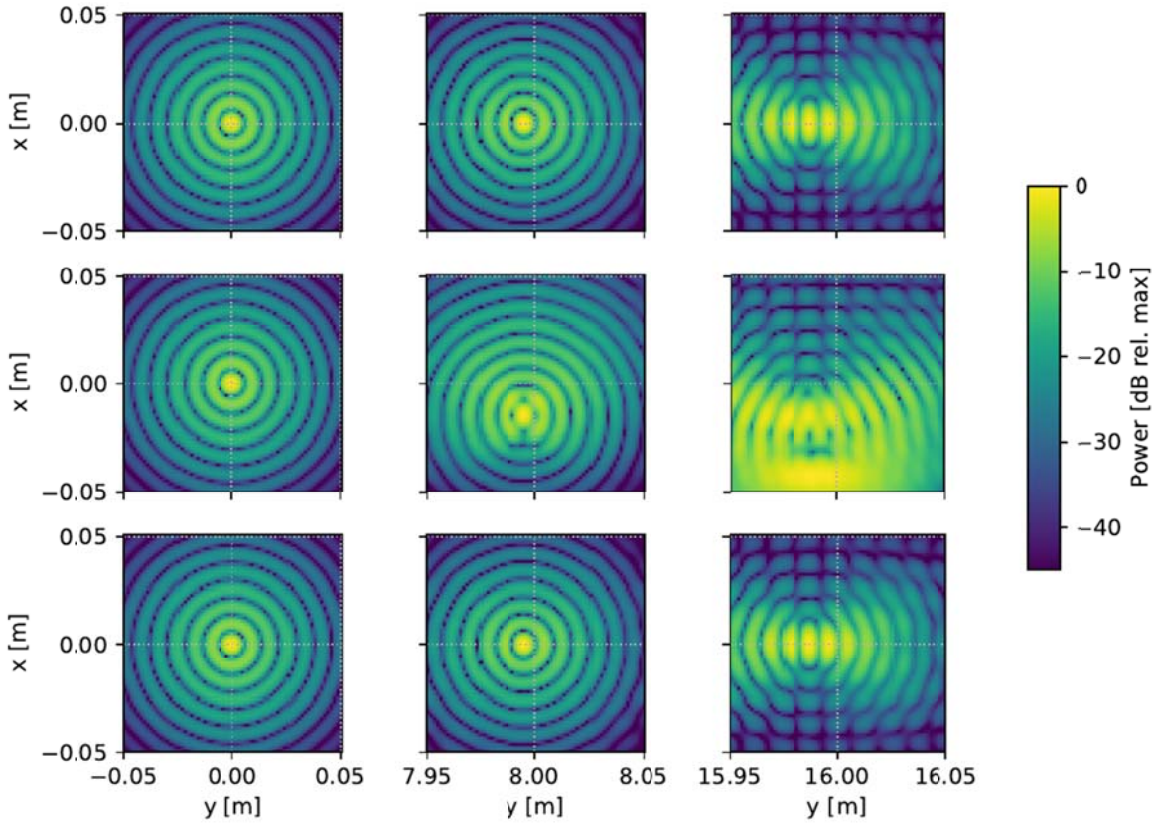

Fig. 1: PSF for three different locations at x_s = 0, and y_s = 5m, 10m, and 16m. Left and centre images are inside the full view area. Right column is outside full view area with apparent splitting of PSF into separate peaks. Top row: Ideal case, without temporal Doppler effect. Second row: with temporal Doppler effect in raw data. Third row: after processing with temporal Doppler compensation;
data simulated and processed under SHA for f_0 = 50 kHz, B = 30 kHz, and T = 10 ms. Slight offset in y-direction visible due to slant range beamforming.

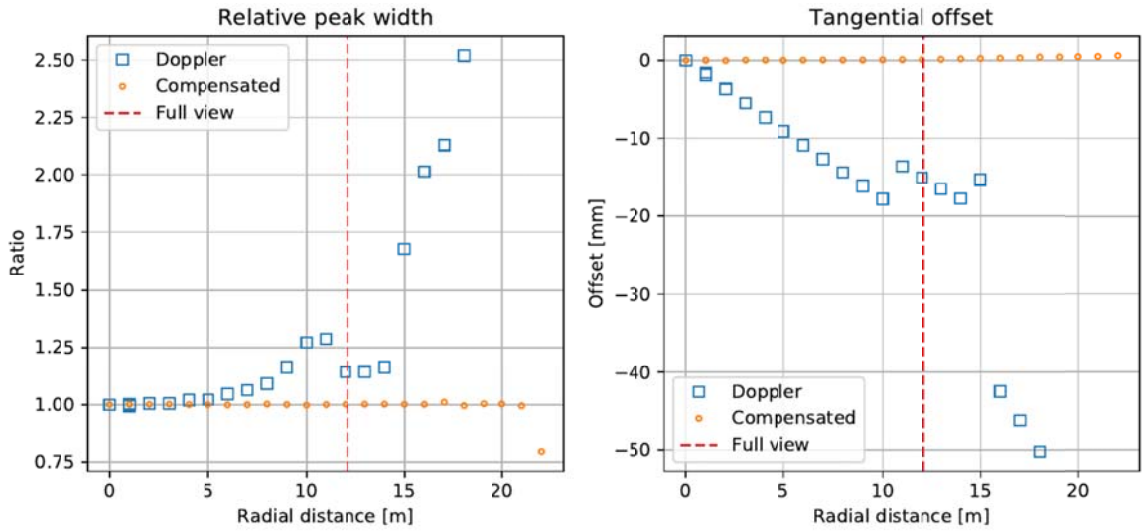

Fig. 2: Impact of temporal Doppler effect on PSF: (a) maximum 6dB peak width relative to the ideal case and (b) tangential offset vs. scatterer radial distance; data simulated and processed under SHA for f_0 = 50 kHz, B = 30 kHz, and T = 10 ms.

Figure 1 shows simulation results for the PSF at x_s = 0, and y_s = 5 m, 10 m, and 16 m, respectively (data simulated and processed under SHA for f_0 = 50 kHz, B = 30 kHz, and T = 10 ms). Left and centre cases are inside the full view area (fully insonified along complete trajectory around centerpoint at (0, 0)) whereas the right case is located outside the full view area with apparent splitting of the PSF into separate peaks. Top row: Ideal case, without temporal Doppler effect in raw data. Second row: with temporal Doppler effect in raw data and processing without temporal Doppler compensation. Third row: with temporal Doppler effect in raw data and processing with compensation for temporal Doppler effect. As expected, there is no impact of the temporal Doppler effect on the central point of the trajectory. There is an apparent increasing tangential shift of the PSF into the forward direction of the trajectory as well as an increasing blurring with rising distance to the central point. The sign of the tangential offset and, thus, its direction will change in case a down-chirp LFM waveform is used. Outside the full view area a quantitative evaluation of shift and blurring will become more and more difficult. However, when applying the compensation scheme for temporal Doppler as described above, the resulting PSF is retrieved almost perfectly even outside the full view area. No tangential offset or degradation of the peaks are visible. This will be analyzed in the following.

Figure 2 shows simulation results for the impact of the temporal Doppler effect on (a) the maximum 6 dB peak width of the PSF relative to the ideal case and (b) the tangential offset of the PSF into the forward direction of the trajectory vs. scatterer radial distance. At the edge of the full view area and outside of it our algorithm to determine the parameters width and shift of the peak of the PSF may fail to provide appropriate results due to the structure of the interference patterns visible in Fig. 1 right column. However, the compensation scheme is shown to be very successful to retrieve the original values for peak width and mitigates the shift almost perfectly even outside the full view area.

In a similar plot the variation with centre frequency, bandwidth, and pulse length is shown (Fig. 3). The impact of the center frequency on the relative 6 dB peak width of PSF is most obvious. This is for two reasons: The normalization relative to the 6 dB peak width in the ideal case without the impact of the temporal Doppler effect causes an increased resolution (decreased peak width) with rising carrier frequency and, secondly, the frequency dependence of the temporal Doppler effect itself. However, the latter one is less prominent as the half power beamwidth (HPBW) of the transducers is reducing with rising carrier frequency which will limit the maximum value of the Doppler shift $|1-\eta| \cdot f_0$. Fig. 4 depicts the two-way Doppler shift $|1-\eta| \cdot f_0$ versus transducer position (phase centre approximation) along the trajectory for a point scatterer at x_s = 10 m and y_s = 0 with parameter centre frequency f_0 = 50 kHz, 75 kHz, and 100 kHz, respectively. Those sub-apertures with a high relative radial velocity between transducer and scatterer along the trajectory (in our example for transducer positions around 70° and 290°) are blanked out for imaging due to the limited beamwidth for the higher frequency cases f_0 =75 kHz and f_0 =100 kHz. Thus, those cases give not rise to significantly higher Doppler shifts as compared to the case with f_0 = 50 kHz.

Finally, the errors caused by uncompensated temporal Doppler are compared to those caused by the SHA. Fig. 5(a) depicts the maximum 6dB peak width of PSF relative to the ideal case and Fig. 5(b) the tangential offset vs. scatterer radial distance for the two cases uncompensated SHA (ignoring temporal Doppler) and uncompensated temporal Doppler effect (SHA for data collection and processing). For the example considered (f_0 = 50 kHz, B = 30 kHz, and T = 10 ms), the blurring caused by uncompensated temporal Doppler is increasing significantly higher with rising scatterer radial distance than that caused by the impact of uncompensated SHA. The tangential offset is almost twice as high but of opposite direction.

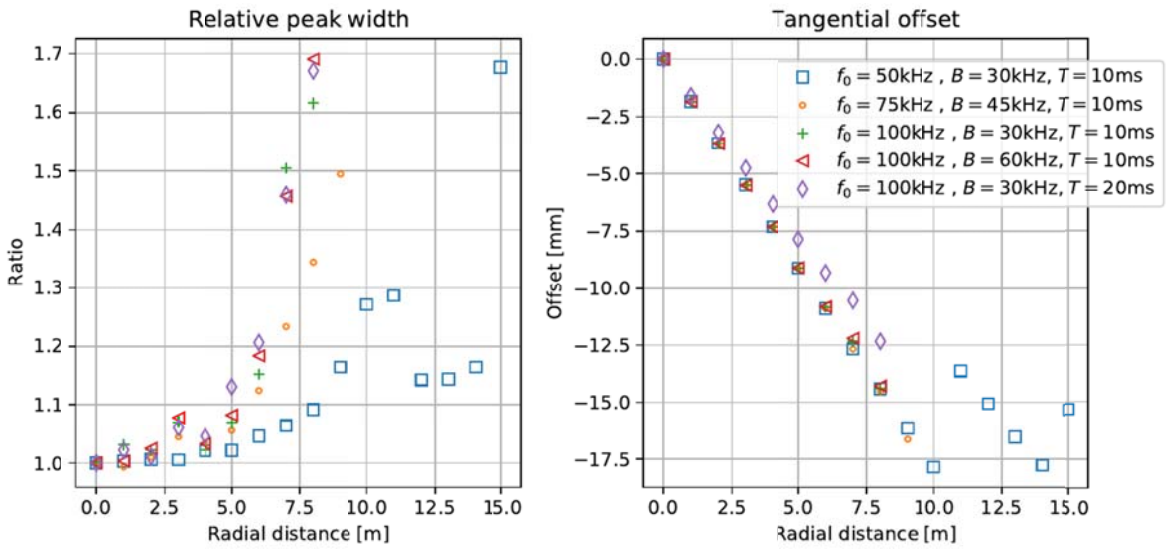

Fig. 3: Comparison of blurring and geometrical shift for various values of f_0, B, and T: (a) maximum 6dB peak width of PSF relative to the ideal case and (b) tangential offset vs. scatterer radial distance; data simulated and processed under SHA.

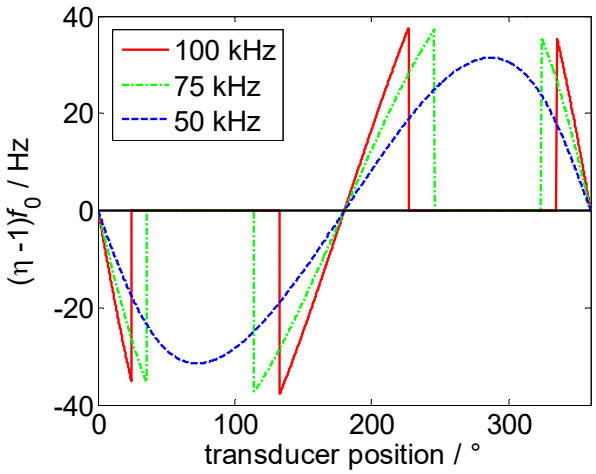

Fig. 4: Two-way Doppler shift $|1-\eta|\cdot f_0$ vs. transducer position along trajectory for point scatterer at x_s = 10 m and y_s = 0 with parameter centre frequency f_0 = 50 kHz ($\theta_b = 45°$), 75 kHz ($\theta_b = 30°$), and 100 kHz ($\theta_b = 22.5°$); transducer position rotating counterclockwise with origin at positive y-axis.

4. DISCUSSION AND CONCLUSION

Due to their high resolution CSAS systems suffer from Doppler time scaling effects. In particular higher speed, multiple receiver CSAS sonars should employ temporal Doppler compensation. The impact of uncompensated temporal Doppler for a LFM waveform and for time-domain processing with SHA was investigated by simulations. Broadening of the 6 dB peak width of the PSF relative to the case where the impact of the temporal Doppler effect was neglected is increasing significantly with rising carrier frequency. On the other hand there is no strong carrier frequency dependence of the temporal Doppler induced tangential shift of the maximum of the PSF. The blurring caused by uncompensated temporal Doppler is

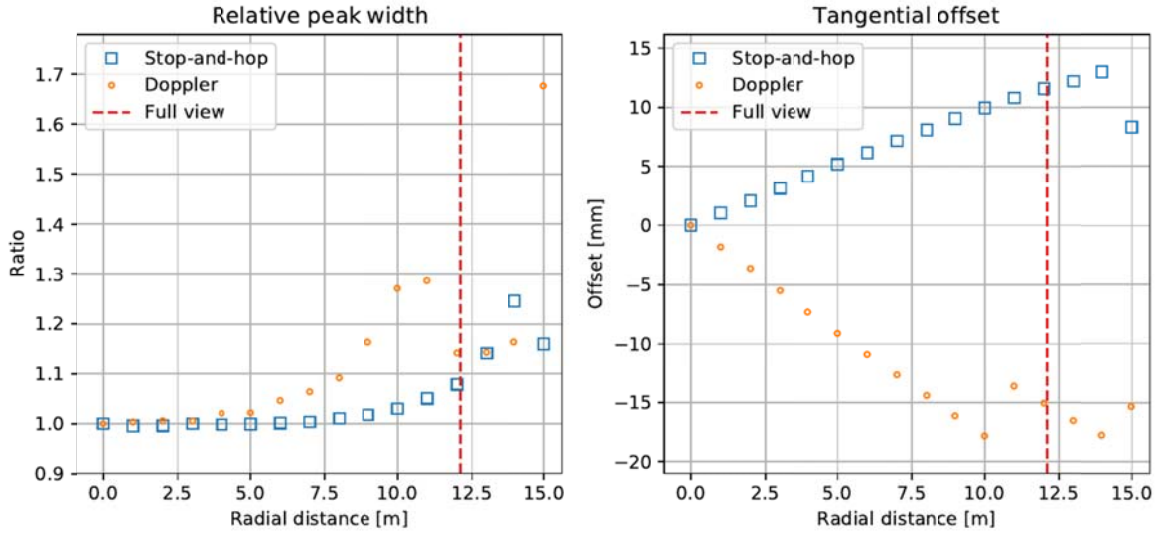

Fig. 5: Comparison of blurring and geometrical shift solely due to uncompensated SHA and solely due to uncompensated temporal Doppler effect: (a) maximum 6dB peak width of PSF relative to the ideal case and (b) tangential offset vs. scatterer radial distance; f_0 = 50 kHz, B = 30 kHz, and T = 10 ms.

increasing significantly higher with rising radial scatterer distance than the blurring caused by the impact of uncompensated SHA. The tangential offset is almost twice as high and in same direction when using a down-chirp waveform (opposite direction for up-chirp waveform). The computational efficient compensation scheme presented was proven to be very successful in removing the tangential offset (image distortion) as well as the blurring during reconstruction of the images. An investigation of the degradation caused by the impact of uncompensated temporal Doppler for the non-SH case (collection and processing) is underway.

ACKNOWLEDGEMENT

This work was supported by Wehrtechnische Dienststelle für Schiffe und Marinewaffen, Maritime Technologie und Forschung (WTD 71), Eckernförde, Germany.

REFERENCES

[1] **T. M. Marston and J. L. Kennedy**, Volumetric acoustic imaging via circular multipass aperture synthesis, *IEEE Journal of Oceanic Engineering*, vol. 41, pp. 852–867, Oct 2016.

[2] **H. Callow, R. Hansen, S. Synnes, and T. Sæbø**, Circular synthetic aperture sonar without a beacon, *Proc. Underwater Acoustic Measurements (UAM)*, 2009.

[3] **U.J. Herter, H. Schmaljohann, and T. Fickenscher**, Impact and limitations imposed by stop-and-hop approximation on CSAS imagery, *UACE 2017 Conference Proceedings*, pp. 561–567, 2017.

[4] **D. Hawkins, P. Gough**, Temporal Doppler effects in SAS, *Proceedings of the Institute of Acoustics*, Vol. 26, Pt. 5, 2004.

[5] **Y. Pailhas, S. Dugelay, and C. Capus**, Impact of temporal Doppler on synthetic aperture sonar imagery, *The Journal of the Acoustical Society of America*, vol. 143, pp. 318–329, 2018.

[6] **A. Ishimaru, T.-K. Chan, and Y. Kuga**, An imaging technique using confocal circular synthetic aperture radar, *IEEE Transactions on Geoscience and Remote Sensing*, vol. 36, pp. 1524–1530, 1998.

[7] **L. Kou, X. Wang, M. Zhu, J. Chong, and M. Xiang**, Resolution analysis of circular SAR with partial circular aperture measurements, *8th European Conference on Synthetic Aperture Radar*, pp. 1–4, June 2010.